Available online at www.sciencedirect.com
SCIENCE DIRECT®
Journal of Solid State Chemistry 177 (2004) 1559–1566
JOURNAL OF SOLID STATE CHEMISTRY
http://elsevier.com/locate/jssc

Mechanosynthesis and mechanical activation processes to the preparation of the $Sr_2[Sr_{n-1}Ti_nO_{3n+1}]$ Ruddlesden–Popper family

Teresa Hungría,[a] Ana-Belén Hungría,[b] and Alicia Castro[a,*]

[a] *Instituto de Ciencia de Materiales de Madrid, CSIC, Cantoblanco, 28049 Madrid, Spain*
[b] *Instituto de Catálisis y Petroleoquímica, CSIC, Cantoblanco, 28049 Madrid, Spain*

Received 18 September 2003; received in revised form 1 December 2003; accepted 9 December 2003

Abstract

A novel mechanochemical activation route has been applied in order to obtain the $n=1$–4 and ∞ members of the $Sr_2[Sr_{n-1}Ti_nO_{3n+1}]$ Ruddlesden–Popper series. The evolution of the $(n+1)SrO{:}nTiO_2$ powder mixtures during mechanical treatment was followed by X-ray powder diffraction in all cases. Except for the $2SrO{:}TiO_2$ composition, $SrTiO_3$ was always mechanosynthesized. High-energy milling of $2SrO{:}TiO_2$ sample resulted in the formation of nanosized Sr_2TiO_4, which is the only K_2NiF_4-type oxide prepared by mechanical treatment until now.

The mechanical treatment was followed by annealing at different temperatures to establish the optimized protocol for synthesis of each member of the series. $SrTiO_3$, Sr_2TiO_4 and $Sr_3Ti_2O_7$ were obtained with very important decreases in the formation temperatures and reaction times as compared with the traditional ceramic method. Final and milled products were studied by X-ray powder diffraction at room and increasing temperatures, and by thermal analysis and scanning and high resolution transmission electron microscopy.

Keywords: Mechanosynthesis; Ruddlesden–Popper; Strontium–titanium oxides; Perovskite

1. Introduction

About 50 years ago, Ruddlesden and Popper described a structural type constructed from $[A_{n-1}B_nO_{3n+1}]$ perovskite-like blocks n octahedra thick, interleaved with A cations along one of the cubic directions of the perovskite structure, yielding phases with the general formula $A_2[A_{n-1}B_nO_{3n+1}]$ where $1 \leqslant n \leqslant \infty$ [1,2] (Fig. 1). The electric transport and magnetic properties of these layered-structure phases are governed by the nature and size of the cations at the sites A and B, the width of n perovskite slabs, the B–O–B angle and the oxygen content [3]. These perovskite-layered compounds present a wide range of applications such as magnetic materials [4] and high-temperature superconductors [5], among others.

The $Sr_2[Sr_{n-1}Ti_nO_{3n+1}]$ series constitute the prototype of the Ruddlesden–Popper phases. The upper end member of the series is the $SrTiO_3$ perovskite ($n=\infty$), whose electrical behavior goes from a high-dielectric-constant material to a metallic superconductor when doped with a variety of elements [6]. The lower end member is Sr_2TiO_4 ($n=1$, K_2NiF_4-type structure), which has good properties for substitution/insertion reactions and can be used to synthesize the new oxide fluoride $Sr_2TiO_3F_2$ [7]. This member with $n=1$ presents some advantages over $SrTiO_3$ for application in tunable devices and for alternative gate oxide in metal-oxide semiconductor field-effect transistors, MOSFETS [8]. The member corresponding to $n=3$, $Sr_4Ti_3O_{10}$, is reported to exhibit water-splitting photocatalytic activity without any co-catalyst, this activity being drastically increased when NiO_x is loaded onto the Ruddlesden–Popper phase [9]. $Sr_4Ti_3O_{10}$ is normally used as a material in solid oxide fuel cells, exhibiting a high degree of flexibility in manipulating the electrical and transport properties.

These oxides are usually prepared by the conventional ceramic method, but high temperatures and long reaction times are required, yielding phases with inhomogeneous particle sizes and deviations in the

*Corresponding author. Fax: +34-91-372-0623.
E-mail address: acastro@icmm.csic.es (A. Castro).

0022-4596/$ - see front matter © 2003 Elsevier Inc. All rights reserved.
doi:10.1016/j.jssc.2003.12.006

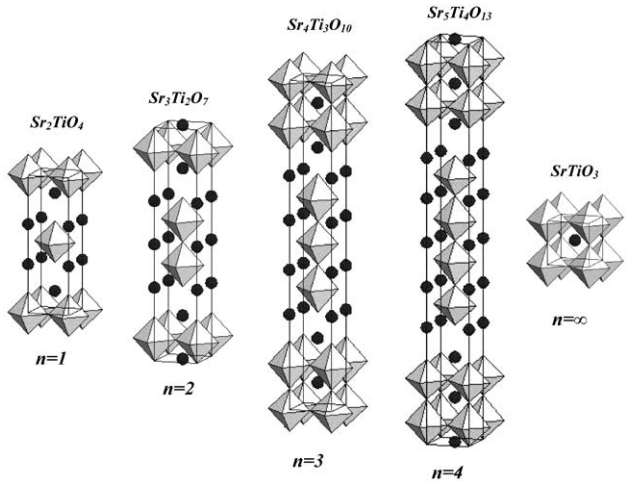

Fig. 1. Unit cells of the members of the $Sr_2[Sr_{n-1}Ti_nO_{3n+1}]$ Ruddlesden–Popper series. Sr atoms are represented by circles, while Ti atoms are at the center of the octahedra TiO_6.

stoichiometry. Thus alternative synthesis routes need to be developed in order to facilitate the successful production of these compounds.

Recently, reactive MBE has been employed to grow thin films of the first five members of the $Sr_2[Sr_{n-1}Ti_nO_{3n+1}]$ homologous series [8,10]. These films are epitaxially oriented and nearly free of intergrowths for $n = 1-3$, but not for $n = 4$ and 5. Interesting electric properties are envisaged from such materials.

Although the first mechanochemical reactions were described at the end of the fourth century B.C. by Theophrastus of Erasus [11], mechanoactivation techniques were developed for the synthesis of intermetallics, alloys and nanocrystalline materials during the 20th century [12–14]. More recently, solid state mechanochemistry has been employed to prepare new oxides, or to improve the properties of known functional materials [15–24]. During the milling process, the homogeneity of the mixture is increased, the particle size decreased and the contact area renewed. Localized heating and the combined action of pressure with shear at the points of impact may contribute to the activation of the milled sample [11]. Mechanochemical activation is usually a result of disordering of the crystal and generation of defects or other metastable forms that cause higher reactivity.

A previous study of the effect of the mechanical activation on the preparation of the $Sr_2[Sr_{n-1}Ti_nO_{3n+1}]$ compounds with $n = 1$, 2 and ∞ has been reported by Berbenni et al. [25]. However, no mechanosynthesis was detected by these authors, although $SrTiO_3$ and Sr_2TiO_4 were obtained after the annealing of stoichiometric, activated mixtures of $SrCO_3$ and rutile. On the contrary, no $Sr_3Ti_2O_7$ could be obtained by similar procedure.

In this paper, we describe an attempt to improve the reaction conditions to obtain the $n = 1-4$ and ∞ members of the $Sr_2[Sr_{n-1}Ti_nO_{3n+1}]$ Ruddlesden–Popper series, decreasing the reaction temperatures and times by mechanical activation of SrO and TiO_2 stoichiometric mixtures, achieved by milling in a planetary system. This method of synthesis was previously optimized for the preparation of the $Sr_3Ti_2O_7$ Ruddlesden–Popper phase [26].

2. Experimental

Stoichiometric mixtures of analytical grade SrO and TiO_2 (anatase) were mixed by hand in an agate mortar, and activated in a planetary mill (Fritsch Pulverisette 6). The initial oxide mixtures were placed in a stainless-steel vessel with five steel balls 2 cm in diameter, the grinding bowl being rotated at 200 rpm. Activated mixtures were finally calcined in one step. Although no special atmospheres were used during grinding, special care was taken with SrO before the milling procedure: it was stored and weighed in a glovebox under controlled nitrogen atmosphere, because of its high instability in air.

The milled powders were characterized by differential thermal analysis (DTA), thermogravimetric analysis (TG), X-ray powder diffraction (XRD) at room and increasing temperatures, and high-resolution transmission electron microscopy (HRTEM). Particle morphology of milled and annealed samples was investigated by scanning electron microscopy (SEM) and microanalysis of the composition was performed by X-ray energy dispersive spectroscopy (XEDS).

XRD patterns at room temperature were measured in a D500 Siemens Diffractometer between 5° and 60° (2Θ), with 2Θ increments of 0.05° and counting time of 0.5 s per step. For high-temperature measurements a Philips PW1310 diffractometer, fitted with an Anton Paar HTK 10 attachment to stabilize the temperature, was used. The patterns were obtained by depositing a small quantity of powder onto a platinum sheet placed on a tantalum strip, which was the heating element. The recordings were taken from 5° to 70° (2θ) with a scan rate of $0.02^\circ\,s^{-1}$. The temperature was monitored by a Pt–Pt 13% Rh thermocouple welded in the center of the platinum sheet. The heating rate was $10^\circ C\,min^{-1}$ and the temperature was stabilized during 1 h. The Cu$K\alpha$ doublet ($\lambda = 0.15418$ nm) was used in all X-ray experiments.

The DTA and TG measurements were taken with a Seiko 320 instrument, with α-Al_2O_3 as the inert reference material, between room temperature and 1200°C at $10^\circ C\,min^{-1}$, in the heating and cooling process, in argon. The evolved gases were analyzed with a Pfeiffer ThermoStar GSD 301 T (quadrupole mass spectrometer) with argon as gas carried to determine the molar mass.

SEM images were taken in the range of 10–20 kV in a Digital Scanning Microscope DSM 960 Zeiss. For this purpose, dispersed particles of the milled and thermally treated powder were placed in a carbon film and a gold layer was sputtered onto it. For XEDS microanalysis a Link Isis Oxford detector was used, and a carbon layer was sputtered on the powder samples.

For transmission electron microscopy studies portions of each sample were crushed in an agate mortar and suspended in *n*-butanol. After ultrasonic dispersion, a droplet was deposited on a copper grid supporting a perforated carbon film. High-resolution electron microscopy (HRTEM) images were recorded in a Philips CM200 FEG microscope. The micrographs were digitized for image processing and Fourier transforms were utilized to determine interplanar angles and spacings (Digital Micrograph). The digital diffraction patterns (DDPs) included in this work correspond to the log-scaled power spectrum of the Fourier transform of the bidimensional intensity distribution in the digitized images. Lattice fringe spacings have been measured from this DDPs by locating the maximum of intensity within the diffraction spots. Errors associated to these measurements are about ± 0.015 nm for spots in the range 0.2–0.4 nm and about $\pm 5^\circ$ in the measurements of interplanar angles. Program Eje Z [27], was used to interpret this interplanar angles and spacings. This program provided the information about the possible crystallographic orientations (zone axis) of a known crystalline structure. Comparison between crystallographic data obtained from this application with that found experimentally from HRTEM micrographs after DDPs allows us to establish the structural phase and the orientation of the material analyzed.

3. Results and discussion

3.1. $Sr_2[Sr_{n-1}Ti_nO_{3n+1}]$ (n=2, 3, 4 and ∞) phases

Table 1 summarizes the milling process and annealing conditions for the $Sr_2[Sr_{n-1}Ti_nO_{3n+1}]$ Ruddlesden–Popper phases with $n = 1$, 2, 3, 4 and ∞ (hereafter referred to as ST1, ST2, ST3, ST4 and ST0, respectively), as well as the products obtained. For all compositions, two steps can be observed during the milling process: first a diminution in particle size of the starting materials, and second a solid-state reaction in the activated mixture, which leads to the formation of nanocrystalline phases. Figs. 2a and b show the XRD pattern evolution for increasing milling times of the mixtures $3SrO{:}2TiO_2$ ($n = 2$) and $SrO{:}TiO_2$ ($n = \infty$), respectively. The diffraction peaks of ST0 can be observed after 50 h of grinding in $n = 2$ and 35 h in $n = \infty$ samples, and further milling produces in both activated mixtures an increase in the ST0 crystallinity. Similar results were obtained when the reactants for $n = 3$ and 4 members were mechanically activated. In all cases $SrTiO_3$ was mechanosynthesized and it was the unique detectable phase after 125 h of milling, remaining stable after longer milling times. In general, it can be said that higher n values imply shorter perovskite synthesis times.

Table 1
Identified phases after mechanical treatment in a planetary mill and thermal annealings of different $SrO{:}TiO_2$ mixtures

T (°C)(t/h)	Milling time (h)						
	0	35	50	70	90	125	300
$n = 1$, $2SrO{:}TiO_2$							
RT	M	M	M	M + ST1tr	ST1lc	ST1lc	ST0
800(6)						ST1	ST1
$n = 2$, $3SrO{:}2TiO_2$							
RT	M	M	M + ST0lc	ST0lc	ST0lc	ST0	ST0
800(24)						ST2	
$n = 3$, $4SrO{:}3TiO_2$							
RT	M	M + ST0tr	ST0lc	ST0	ST0	ST0	ST0
1200(4)				ST3 + ST0tr		ST3 + ST0tr	
$n = 4$, $5SrO{:}4TiO_2$							
RT	M	M + ST0tr	ST0lc	ST0	ST0	ST0	ST0
1300(14)				ST4 + ST0		ST4 + ST0	
$n = \infty$, $SrO{:}\ TiO_2$							
RT	M	ST0lc	ST0lc	ST0	ST0	ST0	ST0

M = mixture of reactants, ST0 = $SrTiO_3$, ST1 = Sr_2TiO_4, ST2 = $Sr_3Ti_2O_7$, ST3 = $Sr_4Ti_3O_{10}$, ST4 = $Sr_5Ti_4O_{13}$, lc = low crystallinity, tr = traces and RT = room temperature.

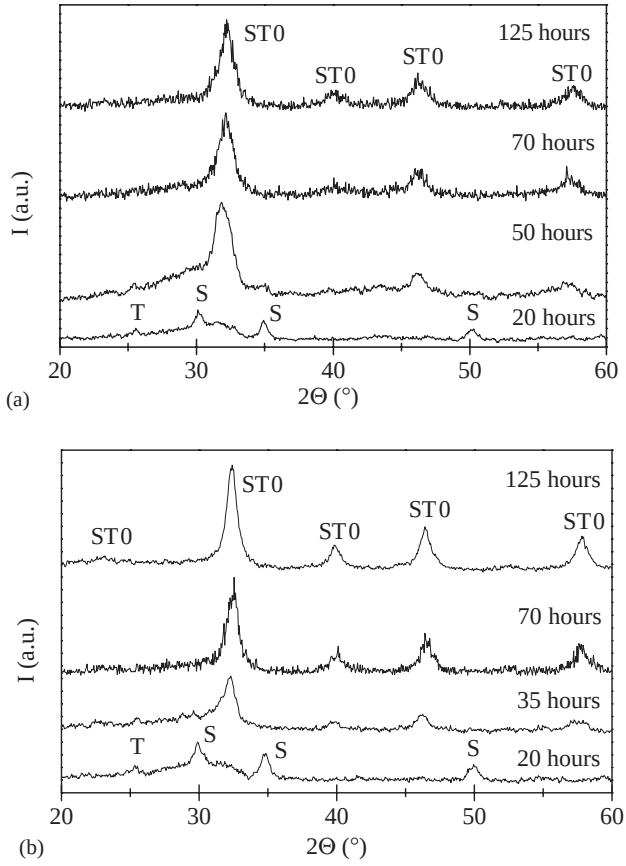

Fig. 2. XRD patterns of the (a) $3SrO:2TiO_2$ and (b) $SrO:TiO_2$ after different mechanochemical activation times (S = SrO, T = TiO_2 and ST0 = $SrTiO_3$).

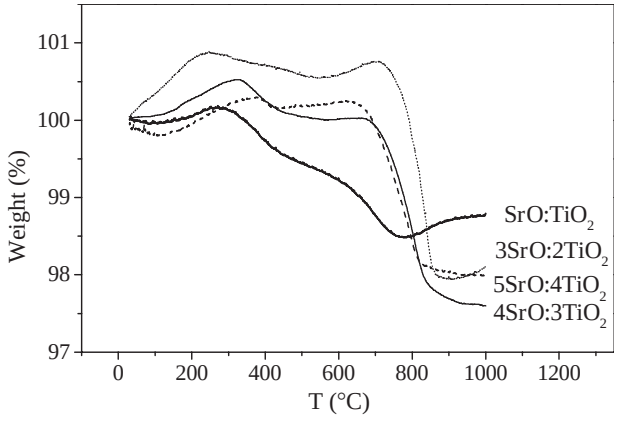

Fig. 3. TG tracings of the different $(n+1)$ $SrO:nTiO_2$ milled mixtures, ($n = 2, 3, 4$ and ∞).

Fig. 3 shows the TG curves of the milled powders for mixtures with $n = 2, 3, 4$ and ∞. The samples chosen for this study present the $SrTiO_3$ perovskite as unique crystalline phase. The thermal behavior of $3SrO:2TiO_2$, $4SrO:3TiO_2$ and $5SrO:4TiO_2$ activated mixtures is very similar, with one small weight increase at low temperature and two weight losses in the temperature ranges 400–600°C and 700–900°C, respectively. The second weight loss is attributed to the elimination of CO_2, as corroborated by mass spectrometric measurements.

When the $SrO:TiO_2$ composition was investigated, a weight increase below 300°C and a two weight losses at 300–600°C and 600–800°C were measured, all of them lower than those in the other compositions. The DTA curves do not exhibit important peaks in any case.

XRD patterns taken at increasing temperatures were brought to bear on the interpretation of TG recordings. In the case of $SrO:TiO_2$ mixture, only an increase of the crystallinity of mechanosynthesized $SrTiO_3$ was observed. Fig. 4 shows XRD patterns of a $3SrO:2TiO_2$ sample milled for 125 h at increasing temperatures. There are no noticeable changes up to 250°C, the perovskite $SrTiO_3$ remaining unchanged. The $SrCO_3$ diffraction lines clearly appear at 600°C, then they disappear at 800°C. Beyond 800°C, the doublet at $2\Theta \approx 31°$, characteristic of $Sr_2[Sr_{n-1}Ti_nO_{3n+1}]$ oxides become observable, although the ST2 phase was not obtained as a single phase, but mixed with the end members of the series (ST0 and ST1).

When $n = 3$ and 4 milled mixtures were studied by XRD at high temperatures, the $SrCO_3$ formation and decomposition were observed at the same temperatures,

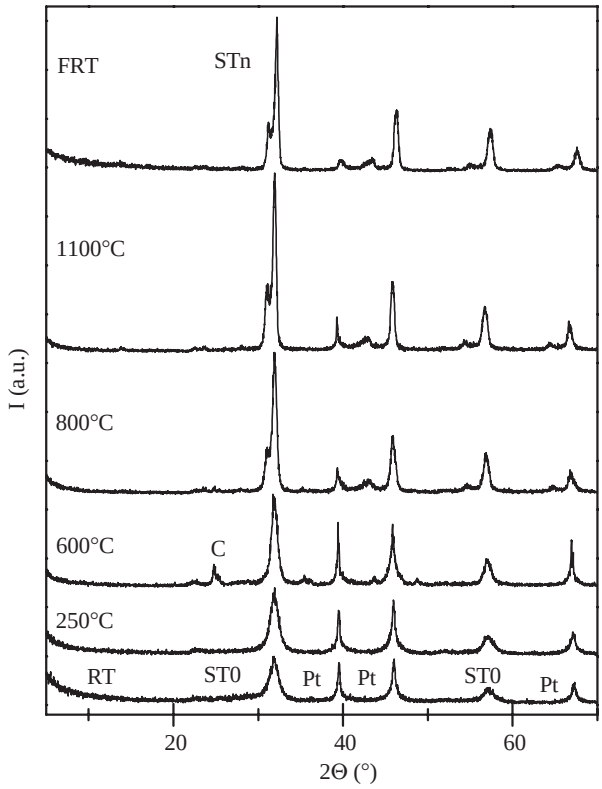

Fig. 4. XRD patterns at increasing temperatures of the $3SrO:2TiO_2$ mixture activated during 125 h (ST0 = $SrTiO_3$, C = $SrCO_3$, Pt = platinum, STn = mixture of different Ruddlesden–Popper phases, RT = room temperature and FRT = final room temperature).

but only a small amount of ST1 is observed, together with the ST0 phase, at temperatures as high as 1100°C. In the case of these members, temperature and time of "in-situ" heating are not high and long enough to obtain the $Sr_4Ti_3O_{10}$ and $Sr_5Ti_4O_{13}$ Ruddlesden–Popper phases.

In order to isolate each stable phase by quenching to room temperature, the activated precursors were heated in a furnace at temperatures similar to those used in the high temperature XRD technique for each composition, but for longer times. The crystallographic transformations were analogous to those above mentioned. For ST2, ST3 and ST4 the results obtained are very similar. No changes are observed when activated samples were heated up to 250°C. As the temperature was further increased, the $SrCO_3$ crystallites grew, and this compound appeared as a very crystalline phase at 600°C, remaining stable up to 800°C, when this phase decomposed by CO_2 elimination, and the expected Ruddlesden–Popper phases are obtained.

The results show that several processes are taking place during both mechanoactivation of the mixtures and annealing treatments, so that the chemical reactions can be understood as follows:

$$(n+1)\mathrm{SrO} + n\mathrm{TiO_2} \xrightarrow{\text{milling}} \mathrm{SrTiO_3} + \text{amorphous phase},$$

$$\mathrm{SrTiO_3} + \text{amorphous phase} \xrightarrow{<250^\circ\mathrm{C}} \mathrm{SrTiO_3} + \mathrm{SrCO_3} + \mathrm{Sr(OH)_2}\cdot n\mathrm{H_2O} + \mathrm{TiO_2},$$

$$\mathrm{SrTiO_3} + \mathrm{SrCO_3} + \mathrm{Sr(OH)_2}\cdot n\mathrm{H_2O} + \mathrm{TiO_2} \xrightarrow{250-800^\circ\mathrm{C}} \mathrm{SrTiO_3} + \mathrm{SrCO_3} + n\mathrm{H_2O}\uparrow,$$

$$\mathrm{SrTiO_3} + \mathrm{SrCO_3} \xrightarrow{800^\circ\mathrm{C}} \mathrm{Sr_2[Sr_{n-1}Ti_nO_{3n+1}]} + \mathrm{CO_2}.$$

After the activation step of the mixtures for $n = 2$, 3 and 4, a small quantity of an amorphous fraction was obtained together with the crystalline perovskite; this fraction contained strontium carbonate and hydroxides with very low crystallinity, formed from SrO which, due to its high instability in air, reacted with CO_2 and moisture of the atmosphere. The crystal size of $SrCO_3$ grew with the temperature, however the hydroxides could not be observed by XRD because decomposition took place at low temperature, before grain growth.

$Sr_3Ti_2O_7$ was obtained as a pure and crystalline phase after a thermal treatment at a temperature as low as 800°C for 24 h, but $Sr_4Ti_3O_{10}$ and $Sr_5Ti_4O_{13}$ could not be isolated as single phase even after annealing at 1300°C (Table 1).

When a SrO:TiO_2 milled mixture was heated, $SrTiO_3$ was the only crystalline phase obtained, and no $SrCO_3$ formation was observed, probably because very little SrO remains as an amorphous phase. The weight loss from 300°C to 800°C might be attributed to the elimination of small quantities of H_2O and CO_2, when formation of the perovskite occurred from the minority amorphous fraction produced during grinding step.

The mechanoactivated powder of the SrO:TiO_2 sample was also studied by HRTEM. In order to consider the structural features as representative of the state of the sample, DDPs of different selected areas belonging to several micrographs were studied. A characteristic HRTEM micrograph is shown in Fig. 5. Fringe analysis of the selected area using Fourier analysis, inset in the same figure, reveals the presence of lattice spacings in the 0.27–0.28 nm range with interplanar angles of 60° corresponding to $(1\bar{1}0)$, $(\bar{1}01)$ and $(0\bar{1}1)$ planes of $SrTiO_3$ structure oriented along the [111] zone axis. Fig. 6 shows the particle size distribution

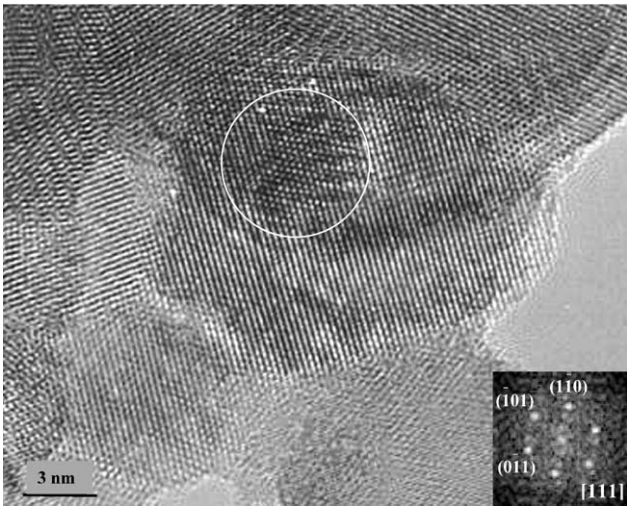

Fig. 5. HRTEM micrograph of the SrO:TiO_2 mixture mechanoactivated for 72 h. Inset: DDP of the selected area.

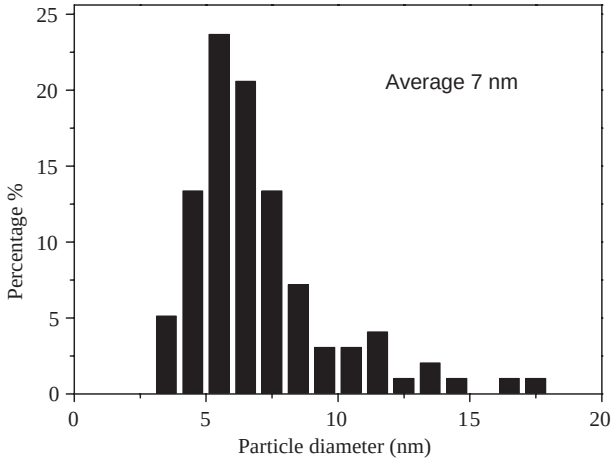

Fig. 6. Particle size distribution from HRTEM micrographs of $SrTiO_3$ mechanosynthesized from the SrO:TiO_2 mixture.

of this nanosized sample obtained by Feret's diameter [28], 95% of the studied particles have a diameter smaller than 15 nm, and the average value is 7 nm.

3.2. Sr_2TiO_4 phase

In the particular case of the $2SrO:TiO_2$ mixture, the milling process produced the mechanosynthesis of Sr_2TiO_4 with very low crystallinity (Fig. 7). It is worthwhile to note that this is, to the best of the authors knowledge, the first K_2NiF_4-type structure to be mechanosynthesized, while several three-dimensional perovskites can be prepared by direct mechanical treatment, for example lead zirconate-titanate (PZT) [29] and lead zinc niobate-lead magnesium niobate-lead titanate (PZN-PMN-PT) [18].

The crystallinity achieved in this case was lower than that of ST0 obtained by mechanosynthesis. Further milling produced the transformation of Sr_2TiO_4 into $SrTiO_3$, therefore the amorphous fraction must be enriched in the strontium components. This result suggests that the cubic perovskite is more stable during the grinding step than is the K_2NiF_4-type structure.

The thermal behavior of the $2SrO:TiO_2$ mixture milled during 125 h (Fig. 8), formed mainly by Sr_2TiO_4, is similar to that of the other mixtures, but the weight variations observed are larger, which might be due to the higher amount of SrO which reacted with the moisture and CO_2 of air. The mass spectrometer measurement of the sample confirms the H_2O and CO_2 elimination between 300°C and 600°C and at 800°C, respectively (Fig. 8).

The XRD patterns at increasing temperatures (Fig. 9) displayed no noticeable differences between the as-milled powders and those subsequently annealed at 200°C. At 400°C the diffraction peaks of $SrCO_3$ begin to be detectable and its crystallite size grew up to 600°C. The formed $SrCO_3$ decomposed at 800°C and Sr_2TiO_4 became more crystalline. The final room temperature pattern shows that the sample was composed by only the ST1 phase with very high crystallinity.

Very similar results were obtained when the activated $2SrO:TiO_2$ sample was annealed, but in this case a small amount of $SrTiO_3$ was observed at 600°C. Sr_2TiO_4 was obtained as a single phase after one furnace treatment at 800°C for 10 h. The sequence of reactions in this

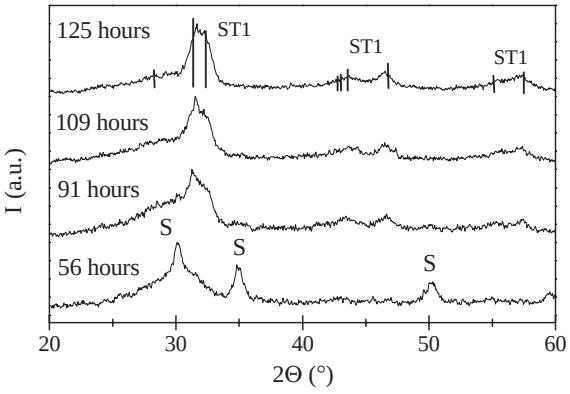

Fig. 7. XRD patterns for the $2SrO:TiO_2$ mixture milled for different times. (S = SrO, ST1 = Sr_2TiO_4, lines correspond to Sr_2TiO_4 (JCPDS 39-1471)).

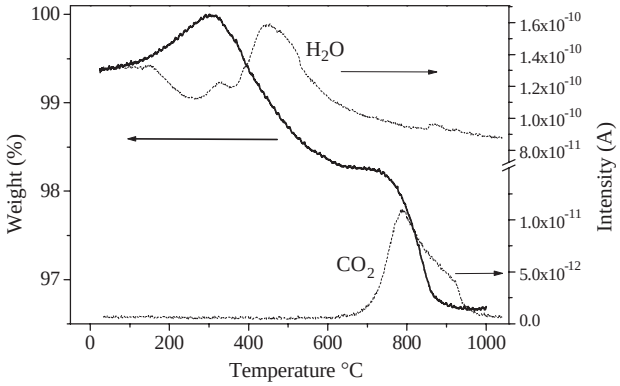

Fig. 8. TG tracing and QMS measurements for masses corresponding to H_2O and CO_2, for the mixture $2SrO:TiO_2$ mechanoactivated during 125 h.

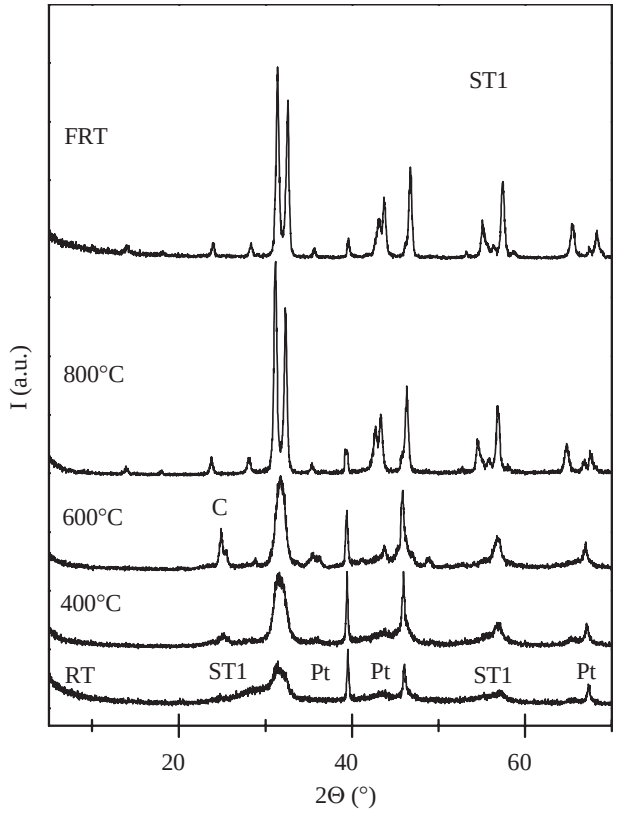

Fig. 9. XRD patterns at increasing temperatures of the $2SrO:TiO_2$ mixture activated during 125 h (Pt = platinum, C = $SrCO_3$, ST1 = Sr_2TiO_4, RT = room temperature and FRT = final room temperature).

composition are:

$$2SrO + TiO_2 \xrightarrow{\text{milling}} Sr_2TiO_4 + \text{amorphous},$$

$$Sr_2TiO_4 + \text{amorphous} \xrightarrow{<400^\circ C} Sr_2TiO_4 + SrCO_3 + Sr(OH)_2 \cdot nH_2O + SrTiO_3,$$

$$Sr_2TiO_4 + SrCO_3 + Sr(OH)_2 \cdot nH_2O + SrTiO_3 \xrightarrow{400-600^\circ C} Sr_2TiO_4 + SrCO_3 + nH_2O\uparrow + SrTiO_3,$$

$$Sr_2TiO_4 + SrCO_3 + SrTiO_3 \xrightarrow{800^\circ C} Sr_2TiO_4 + CO_2.$$

The Sr_2TiO_4 phase formation was triggered during the activation process together with some amorphous fraction, which reacted in the same way as for the other mixtures. $SrTiO_3$ was observed as an intermediate compound between 600°C and 800°C.

The $2SrO:TiO_2$ activated mixture was investigated by HRTEM to make a comparative study with the perovskite obtained by mechanical activation of the other oxide mixtures. Fig. 10 is a representative micrograph showing a periodic stacking sequence seen in several regions of this sample. Fourier analysis of these zones shows d-spacings about 0.28 nm and 0.63 nm assigned to (103) and (002) planes of Sr_2TiO_4 phase (SPG $I4/mmm$) viewed in the direction of the [010] zone axis. The spacing of the stacking sequence is 1.26 nm (indicated by arrows in the Fig. 10) and it reproduces exactly the c parameter of the tetragonal unit cell.

Particle size distribution in the sample can be observed in Fig. 11. The average diameter is 7 nm, the same as that obtained in the case of mechanosynthesized

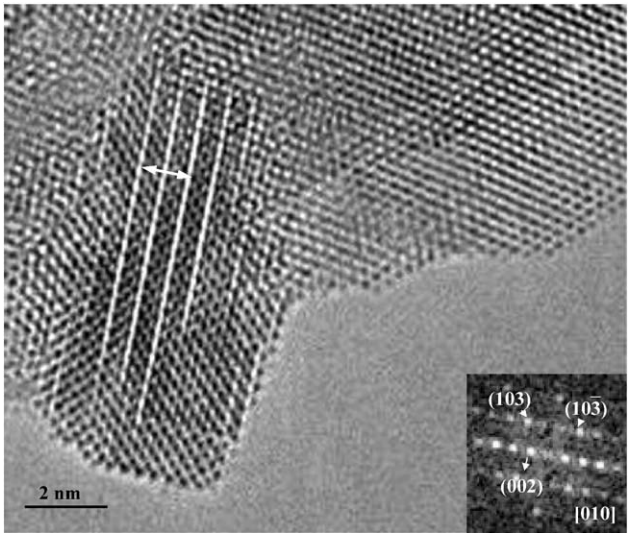

Fig. 10. HRTEM micrograph of the $2SrO:TiO_2$ mixture mechanoactivated for 125 h. Inset: DDP of the periodic stacking zone (the spacing, indicated by arrows, is 1.26 nm).

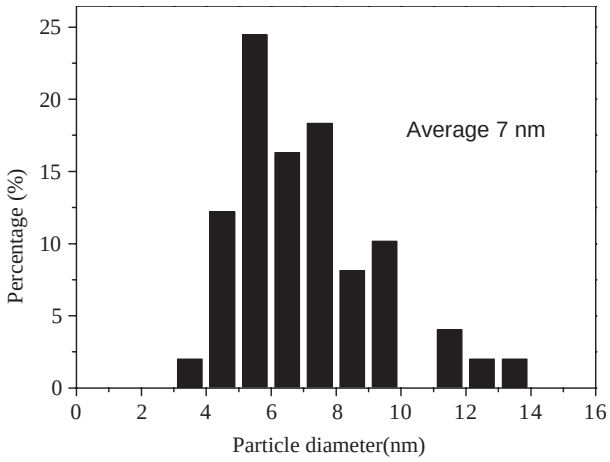

Fig. 11. Particle size distribution from HRTEM micrographs of $2SrO:TiO_2$ mixture mechanoactivated during 125 h.

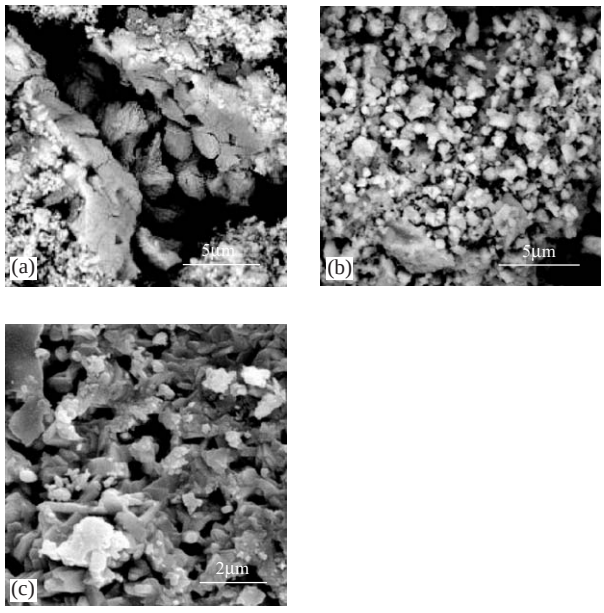

Fig. 12. Scanning electron micrographs of (a) initial $2SrO:TiO_2$ mixture and $5SrO:4TiO_2$ milled mixture unannealed, (b) and annealed at 1300°C for 14 h (c).

$SrTiO_3$, and no particles with a diameter larger than 14 nm were observed.

3.3. Comparative morphological characterization

The morphological characteristics of all compositions were investigated by SEM, after both milling and annealing treatments. Fig. 12 shows the example of the evolution of the morphology in the case of the $5SrO:4TiO_2$ mixture. The initial powders (Fig. 12a) consisted of two grain types: spherical particles with diameters between 50 and 100 nm and larger grains, with rough surfaces and sizes between 2 and 5 μm,

corresponding to TiO_2 and SrO particles, respectively. In the scanning electron micrographs of the activated mixture two kinds of particles can be observed: conglomerates of fine grains with spherical shape 200–400 nm in size, and large grains (3–7 μm in size) with crystalline aspect.

When the composition of the activated mixtures were investigated by XEDS, similar Sr and Ti contents were found in several zones, and the Sr:Ti ratio was close to the nominal compositions. This indicates the presence of mechanosynthesized Sr–Ti oxides in all of the milled sample. On the contrary, when contamination of the samples through the mechanical treatment was studied by XEDS, only about 0.1 at% iron was detected for very long milling times. The iron is oxidized forming Fe_2O_3 in very small quantity, so negligible incidence on the final products is expected.

The annealed samples chosen for the morphological characterization were those obtained by the optimized protocol for the synthesis of each Ruddlesden–Popper member. The changes in the morphology of the sample after annealing treatments depend on time and temperature. The biggest change is observed in the image of the mixture $5SrO{:}4TiO_2$ after annealing at 1300°C for 14 h (Fig. 12c). The annealed powder is very homogeneous and is composed of crystals with irregular shape and size between 200 and 900 nm.

4. Conclusions

The mechanochemical activation of the different $(n+1)SrO{:}nTiO_2$ mixtures involves a very important decrease in temperature (300°C in average) and reaction time (several days) in the synthesis of the members of $Sr_2[Sr_{n-1}Ti_nO_{3n+1}]$ Ruddlesden–Popper series. This is a consequence of the fracture of the grains and defects generated during grinding, which leads to a higher internal energy and reduces the thermal barrier for any subsequent reaction.

The mechanosynthesis of $SrTiO_3$ was observed during the milling process for $SrO{:}TiO_2$, $3SrO{:}2TiO_2$, $4SrO : 3TiO_2$ and $5SrO{:}4TiO_2$ compositions. In the case of $2SrO{:}TiO_2$ mixture the formation of ST1 phase was triggered by the mechanical activation process. Sr_2TiO_4 is the first K_2NiF_4-type structure obtained by mechanosynthesis.

The synthesis protocols of $SrTiO_3$, Sr_2TiO_4 and $Sr_3Ti_2O_7$ have been largely improved and these compounds could be isolated as single, crystalline phases after annealing at temperatures as low as 800°C. In the case of $Sr_4Ti_3O_{10}$ and $Sr_5Ti_4O_{13}$, the formation temperature was also decreased, but members with $n = 3$ and 4 could not be isolated, which can be due to the intergrowths with other members of the series, as the high resolution electron microscopy studies, now in progress, appear to indicate.

Acknowledgments

This work was funded by projects MAT 2001-0561 and CAM 07N/0076/2002. The authors thank Prof. J.E. Iglesias for many valuable discussions and help with the final version of the manuscript. T.H. thanks the MECD of Spain for the postgraduate FPU grant awarded (AP2000-3477). A.-B.H. gratefully acknowledges the CAM for a postgraduate grant. SEM and HRTEM work have been carried out at the Centro de Ciencias Medioambientales (CSIC) and the Centro de Microscopía Electrónica "Luis Bru" (Universidad Complutense de Madrid), respectively.

References

[1] S. Ruddlesden, P. Popper, Acta Crystallogr. 10 (1957) 538–539.
[2] S. Ruddlesden, P. Popper, Acta Crystallogr. 11 (1958) 54–55.
[3] I. Sharma, D. Singh, Bull. Mater. Sci. 21 (1998) 363–374.
[4] R. Mahesh, R. Mahendiran, A. Raychaudhuri, C. Rao, J. Solid State Chem. 122 (1996) 448–450.
[5] R. Cava, R. van Dover, B. Batlogg, E. Rietman, Phys. Rev. Lett. 58 (1987) 408–410.
[6] Y. Wang, W. Zhong, C. Wang, P. Zhang, Solid State Commun. 120 (2001) 133–136.
[7] P. Slater, R. Gover, J. Mater. Chem. 12 (2002) 291–294.
[8] J. Haeni, C. Theis, D. Schlom, W. Tian, X. Pan, H. Chang, I. Takeuchi, X. Xiang, Appl. Phys. Lett. 78 (2001) 3292–3294.
[9] Y-.G. Ko, W. Lee, Catal. Lett. 83 (2002) 157–160.
[10] W. Tian, X. Pan, J. Haeni, D. Scholm, J. Mater. Res. 16 (2001) 2013–2026.
[11] V. Boldyrev, K. Tkacova, J. Mater. Synth. Process. 8 (2000) 121–131.
[12] J. Benjamin, Sci. Am. 234 (1976) 40–49.
[13] J. Ding, W. Miao, P. McCormick, R. Street, Appl. Phys. Lett. 67 (1995) 3804–3806.
[14] A. Giri, Adv. Mater. 9 (1997) 163–166.
[15] A. Castro, P. Millán, L. Pardo, B. Jiménez, J. Mater. Chem 9 (1999) 1313–1317.
[16] A. Castro, P. Millán, J. Ricote, L. Pardo, J. Mater. Chem. 10 (2000) 767–771.
[17] E. Brzozowski, M. Castro, J. Eur. Ceram. Soc. 20 (2000) 2347–2351.
[18] D. Wan, J. Xue, J. Wang, J. Am. Ceram. Soc. 83 (2000) 53–59.
[19] A. Castro, D. Palem, J. Mater. Chem. 12 (2002) 2774–2780.
[20] L. Pardo, A. Castro, P. Millán, C. Alemany, R. Jiménez, B. Jiménez, Acta Mater. 48 (2001) 2421–2428.
[21] A. Moure, L. Pardo, C. Alemany, P. Millán, A. Castro, J. Eur. Ceram. Soc. 21 (2001) 1399–1402.
[22] J. Lim, J. Xue, J. Wang, Mater. Chem. Phys. 75 (2002) 157–160.
[23] E. Avvakumov, E. Devyatkina, N. Kosova, J. Solid State Chem. 113 (1994) 379–383.
[24] E. Avvakumov, M. Senna, N. Kosova, Soft Mechanochemical Synthesis: A Basics for New Chemical Technologies, Kluwer Academic Publishers, Boston, 2001.
[25] V. Berbenni, A. Marini, G. Bruni, J. Alloys Compd. 329 (2001) 230–238.
[26] T. Hungría, J. Lisoni, A. Castro, Chem. Mater. 14 (2002) 1747–1754.
[27] J.A. Pérez Omil, Tesis Doctoral. Universidad de Cádiz, 1994.
[28] R. Matyi, L. Schwartz, J. Butt, Catal. Rev. Sci. Eng. 29 (1987) 41–99.
[29] Z. Brankovic, G. Brankovic, J. Varela, J. Mater. Sci. Mater Elec. 14 (2003) 37–41.